

1  
2  
3  
4  
5  
6  
7  
8  
9  
10  
11  
12  
13  
14  
15  
16  
17  
18  
19  
20  
21  
22

**Supporting Information for**  
**Detecting seasonal and long-term vertical displacement in the North**  
**China Plain using GRACE and GPS**

Linsong Wang, Chao Chen, Jinsong Du, and Tongqing Wang

Hydrology and Earth System Sciences, 2016

**Section S1. The effects of non-tidal ocean variations and atmospheric loading on the GRACE model and GPS coordinates**

As part of the processing performed by the GRACE Project, the GRACE Stokes coefficients (denoted by the GRACE Project as “GSM” coefficients) have had modeled estimates of the atmospheric and oceanic mass signals removed. Thus the GRACE coefficients include the full effects of terrestrial water storage, but the only remaining atmospheric and oceanic signals are those due to errors in the respective models. The GRACE Project provides the modeled atmospheric and oceanic contributions to the Stokes coefficients in two forms: “GAC” files which include the global atmospheric and oceanic effects, and “GAD” files which have had the atmospheric signals over land set to zero. The coefficients in the GAD file therefore represent ocean bottom pressure variations. “GAA” files are those add CSR's GAC files to the GSM files, and subtract the GAD files. The coefficients in the GAA file represent atmospheric pressure variations.

The cause of the difference between our results and Liu's work [Liu et al., 2014] is that we removed atmospheric and non-tidal ocean loading effects but they did not. The atmospheric and non-tidal ocean were not considered in Liu's paper, in which they used the AOD1B (atmosphere and ocean de-aliasing level-1b) product to add back the de-aliasing atmospheric and non-tidal oceanic effects to the GRACE

23 data, primarily because Liu et al.[2014] think these effects cannot be easily removed from the GPS  
 24 height time series.

25 Taking into account the elastic deformation of the solid Earth under the variable load via the load Love  
 26 number  $k_n$  for loading harmonic of degree  $n$ , we get the final formula:

27

$$C_{nm} = \frac{a^2(1 + k_n)}{(2n + 1)Mg} \iint_{Earth} P_s P_{nm}(\cos\theta) \cos\lambda m dS$$

$$S_{nm} = \frac{a^2(1 + k_n)}{(2n + 1)Mg} \iint_{Earth} P_s P_{nm}(\cos\theta) \sin\lambda m dS$$

The equation (3-7) from GRACE AOD1B Product Description Document [Flechtner, 2007].

28

29 Because in the current approach the de-aliasing ADO1B products are represented by a spherical  
 30 harmonic series of degree and order 100 the following loading Love numbers are used [Dong et al,  
 31 1996; Farrell, 1972]:

32

$$k_0 = 0; \quad k_1 = 0; \quad k_2 = -0.308; \quad k_3 = -0.195; \quad k_4 = -0.132$$

$$k_5 = -0.103; k_6 = -0.089; k_7 = -0.082; k_8 = -0.078; k_9 = -0.073$$

$$\text{for } k_{10} \text{ to } k_{17}: -\frac{0.682 + 0.27(n - 10)/8}{n}$$

$$\text{for } k_{18} \text{ to } k_{31}: -\frac{0.952 + 0.288(n - 18)/14}{n}$$

$$\text{for } k_{32} \text{ to } k_{55}: -\frac{1.24 + 0.612(n - 32)/24}{n}$$

$$\text{for } k_{56} \text{ to } k_{100}: -\frac{1.402 + 0.059(n - 56)/44}{n}$$

The load Love number  $k_n$  for loading harmonic of degree  $n$ , from GRACE AOD1B Product Description  
 Document [Flechtner, 2007].

33

34 In our processing strategy, the AOD1B product was not added back to the GRACE Stokes coefficient,  
35 which means our GRACE-derived loading deformation did not include the atmospheric and non-tidal  
36 ocean effects. In order to remove the effects of atmospheric and non-tidal oceanic loading on the GPS  
37 coordinates, we computed the displacements due to atmospheric loading using data and programs  
38 developed by the GGFC (Global Geophysical Fluid Center) (T. van Dam, NCEP Derived 6 hourly,  
39 global surface displacements at  $2.5^\circ \times 2.5^\circ$  degree spacing, <http://geophy.uni.lu/ncep-loading.html>,  
40 2010), which utilized the NCEP (National Center of Environmental Protection) reanalysis surface  
41 pressure data set. The 12-hour sampling model, ECCO (Estimating the Circulation & Climate of the  
42 Ocean), is used to compute the surface displacement driven by non-tidal ocean effects and its spatial  
43 resolution is  $1^\circ \times 0.3-1.0^\circ$ . The effects of non-tidal ocean variations and atmospheric loading on the  
44 GPS coordinates see the Figure S1.

45 In Liu's work, they added GRACE's Atmosphere and Ocean De-aliasing Level-1B (AOD1B) solution  
46 (GAC solution) to the GRACE spherical harmonic solutions. And they adopt the load Love numbers  
47 from Guo et al. [2004] to transform these coefficients into vertical surface deformation estimates. We  
48 check the two results of Love numbers (ocean-load and atmospheric pressure-load) from Guo et al.  
49 [2004], there are significant differences between ocean-load and atmospheric pressure-load Love  
50 numbers. Meanwhile, we compared  $k_n$  Love numbers from Guo et al. [2004] (Liu et al.'s work) and  $k_n$   
51 Love numbers from Han and Wahr [1995] (our work) with the  $k_n$  Love numbers used in ADO1B  
52 products, respectively.

53 We found  $k_n$  from ocean-load Love numbers [Guo et al., 2004] and  $k_n$  Love numbers from Han and  
54 Wahr [1995] are not identical, but they look pretty close with the  $k_n$  Love numbers used in ADO1B  
55 products. However,  $k_n$  from atmospheric pressure-load Love numbers [Guo et al., 2004] shows a big

56 difference with all other results (Figure S2). So, Liu et al.[2014] probably use the atmospheric  
57 pressure-load Love numbers to calculate the vertical displacements, and this approach leads to the  
58 amplitude of the same station from GRACE much more than GPS and our GRACE results, caused by  
59  $k_n$  from atmospheric pressure-load Love numbers [Guo et al., 2004] significantly larger than Love  
60 numbers from Han and Wahr [1995] and Farrel [1972] (see the Table S2).

61

62 Figure S1(a) shows an example GPS site (BJFS) comparing the GRACE-modeled height displacements  
63 with (add GAD and GAA, shown as blue and red solid line, respectively) and without the AOD1B  
64 model (black solid line). Basing on GRACE solutions without the AOD1B model, the results also show  
65 the difference between the GRACE-modeled height displacements with not destriping (black dashed  
66 line) and after destriping (black solid line). In addition, after destriping and removing GLDAS/Noah  
67 model, GRACE-modeled (without the AOD1B model) height displacements show an obvious rising  
68 trend and the seasonal amplitudes are reduced (green solid line).

69 Figure S1(b) shows an example GPS site (BJFS) comparing GRACE AOD1B product with the effects  
70 of atmospheric and non-tidal ocean loading on the GPS coordinates from the NECP and ECCO data. It  
71 is clear that the effect of atmospheric (red solid line) and non-tidal ocean (blue solid line) loading from  
72 the AOD1B agrees with the NECP-modeled (black cross symbols) and (orange cross symbols) seasonal  
73 variations.

74 Seasonal amplitudes and phases fit of vertical displacements derived by GRACE and GPS for IGS  
75 stations between before and after atmospheric and non-tidal ocean corrected are compared (Table S1).

76 This is achieved by a simultaneous fit for the annual and semi-annual signals. GRACE-modeled  
77 amplitudes and phases of the vertical displacements due to seasonal loading show high correlation with

78 GPS which observed seasonal position variations. This fact confirms that the hydrological and  
79 atmospheric mass cycle is the main cause of seasonal ground deformation in the NCP. When the effects  
80 of atmospheric and non-tidal ocean are removed, both GPS and GRACE show the seasonal  
81 hydrological variations, but amplitude and phase appear to have changes with varying degrees in GPS  
82 and GRACE. This result suggests that GPS measurements can sense the difference between loads very  
83 near the site, and loads a bit further away, but GRACE can not. Thus, the amplitude of GPS basically is  
84 greater than the GRACE data and the phase of different GPS sites shows obvious difference compared  
85 with GRACE. In other words, GRACE underestimates NCP vertical displacements at sites very near  
86 regions of concentrated loads, because GRACE solutions truncate to  $l_{max}=60$ , and so smooth out  
87 concentrated loads.

88

## 89 **Section S2. Comparison between GPS and GRACE-derived seasonal variations**

90 The vertical displacements are computed at the GPS sites from the GRACE-derived gravity field  
91 coefficients and compared with the GPS measurements, and 24 selected stations (CMONOC) are shown  
92 in Figure S3. Besides, the horizontal seasonal (detrended and fit) displacements between GPS observed  
93 and GRACE-derived for site BJFS, BJSH, JIXN, TAIN and ZHNZ are shown in Figure S4. Although  
94 nearly half of the GPS data are missing 4~6 months from 2011 to 2012, we can also find that the  
95 seasonal variations of vertical surface displacement are in both GPS and GRACE solutions.

96 To quantitatively evaluate the consistency of seasonal variation between GPS and GRACE, the relative  
97 correlation coefficients of seasonal variation between GPS and GRACE are computed. We also remove  
98 GRACE-derived seasonal deformation from GPS observed detrended height time series, and compute  
99 the reductions of WRMS (Weighted Root-Mean-Squares) basing on the following equation [van Dam

100 et al., 2007]:

101

$$WRMS_{reduction}(\%) = \frac{WRMS_{GPS_i} - WRMS_{GPS_i-GRACE_i}}{WRMS_{GPS_i}} \times 100$$

102

103 Table S3 shows the correlation between GPS and GRACE derived seasonal variations and WRMS

104 reduction ratio of removing GRACE-derived seasonal deformation from GPS observed detrended

105 height time series (between non-corrected and after atmospheric and non-tidal ocean corrected).

106

### 107 **Section S3. Long-term uplift due to the mass loss and GIA effects**

108 Besides the significant seasonal variations discussed above, there is also a long-term uplift contained in

109 GRACE-derived vertical displacement, which is primarily due to the TWS loss and potential GIA

110 effects in the NCP.

111 Table S3 shows the seasonal amplitudes, phases and trend fit of vertical displacements between derived

112 by GRACE and remove GLDAS-derived deformation from GRACE, the annual and semi-annual

113 amplitude reduced nearly half after remove GLDAS-derived deformation from GRACE, but there is no

114 obvious change for trend rate before and after removing GLDAS-derived deformation.

115 And GIA uplift rate for a compressible Earth was computed (results computed and provided by Geruo

116 A) using the ICE5G ice history and VM2 viscosity profile [Peltier et al., 2004], which assumes a

117 compressible Earth, and includes polar wander feedback, degree-one terms, and a self-consistent ocean.

118 Figure S5 shows GIA effects from GPS measurements, which is about 0.2~0.4 mm/year in the land

119 areas of China (a) and 0.28~0.33 mm/year in the NCP (b).

120

121 **Section S4. Land subsidence in NCP**

122 In order to verify vertical crust movement using the corrected vertical rates after subtracting the  
123 GRACE-derived long-term uplift rate due to load changes and GIA effects, we compare the previous  
124 study results from the vertical crust movement model between 2007-2013 (Figure S5a) [MLR, 2015]  
125 and the vertical motion in north China with high spatial resolution (Figure S5b) [Zhao et al., 2014]. We  
126 find that our study agree with the previous study results which combining with mobile and continuous  
127 GPS observation or leveling data. The results show that there are uplift areas and subsidence areas in  
128 NCP. Almost the whole central and eastern region of NCP suffers from serious ground subsidence,  
129 caused by the groundwater exploitation in the deep confined aquifers. In addition, in the most areas of  
130 Shanxi plateau shows ground uplifts lightly. The results reveal that the present vertical motion pattern  
131 of north China is consistent with neotectonic movement and human activities.

132

133 **References**

- 134 Dong, D., Fang, P., Bock, Y., Cheng, M.K., Miyazaki, S., 2002. Anatomy of apparent seasonal  
135 variations from GPS-derived site position time series. *J. Geophys. Res.* 107(B4), 2075.  
136 <http://dx.doi.org/10.1029/2001JB000573>.
- 137 Farrell, W.E., 1972. Deformation of the Earth by surface loads. *Rev. Geophys. Space Phys.* 10, 761–  
138 797. <http://dx.doi.org/10.1029/RG010i003p00761>.
- 139 Flechtner, F., 2007. GRACE AOD1B product description document for product releases 01 to 04, Tech.  
140 Rep., Rev. 3.1, GRACE Doc. 327–750, GeoForschungsZentrum Potsdam, Potsdam, Germany.
- 141 Guo, J.Y., Li, Y.B., Huang, Y., Deng, H.T., Xu, S.Q., Ning, J.S., 2004. Green's Function of Earth's  
142 Deformation as a Result of Atmospheric Loading. *Geophys. J. Int.*, 159, 53–68.

143 <http://dx.doi.org/10.1111/j.1365-246X.2004.02410.x>.

144 Han, D., and Wahr, J., 1995. The viscoelastic relaxation of a realistically stratified Earth, and a further  
145 analysis of post-glacial rebound. *Geophys. J. Int.*, 120, 287–311.

146 Liu, R.L., Li, J.C., Fok, H.S., Shum, C.K., Li, Z., 2014. Earth surface deformation in the North China  
147 Plain detected by joint analysis of GRACE and GPS data. *Sensors* 14, 19861-19876.  
148 <http://dx.doi.org/10.3390/s141019861>.

149 Ministry of Land and Resources of China (MLR), 2015. *Monitoring results of important geographical*  
150 *conditions in the Beijing-Tianjin-Hebei region*, Ministry of Land and Res. of China, Beijing. [Available  
151 at <http://www.mlr.gov.cn/>].

152 Peltier, W.R., 2004. Global glacial isostasy and the surface of the ice-age earth: The ice-5G (VM2)  
153 model and GRACE. *Annu. Rev. Earth Planet. Sci.* 32, 111-149.

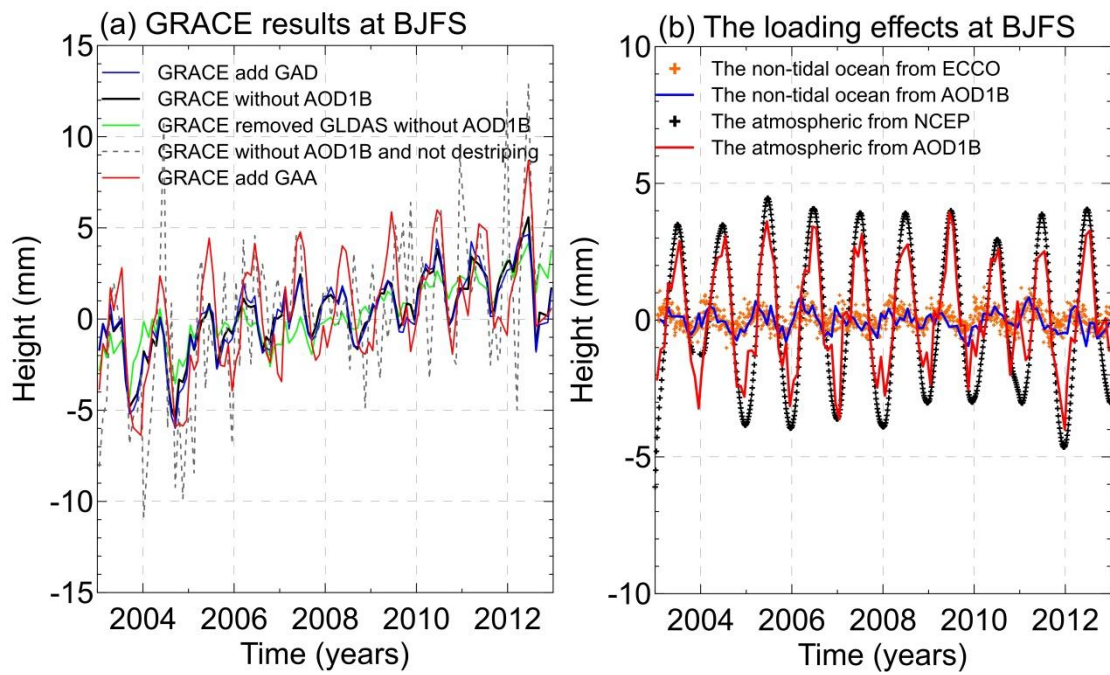
154 van Dam, T., Wahr, J., Lavallée, D., 2007. A comparison of annual vertical crustal displacements from  
155 GPS and Gravity Recovery and Climate Experiment (GRACE) over Europe. *J. Geophys. Res.* 112,  
156 B03404. <http://dx.doi.org/10.1029/2006JB004335>.

157 Zhao, B., Nie, Z.S., Huang, Y., Wang, W., Zhang, C.H., Tan, K., Du, R.L., 2014. Vertical motion of  
158 north China inferred from dense GPS measurements. *J. Geodesy Geodyn.* 34 (5), 35–39 (In Chinese  
159 with English abstract).

160



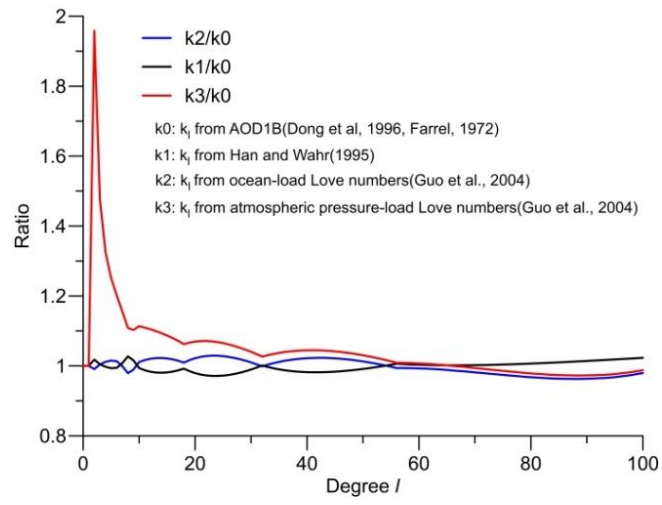
161 **Figure S1.** The effects of non-tidal ocean variations and atmospheric loading on the GRACE model  
162 and GPS coordinates.  
163



164

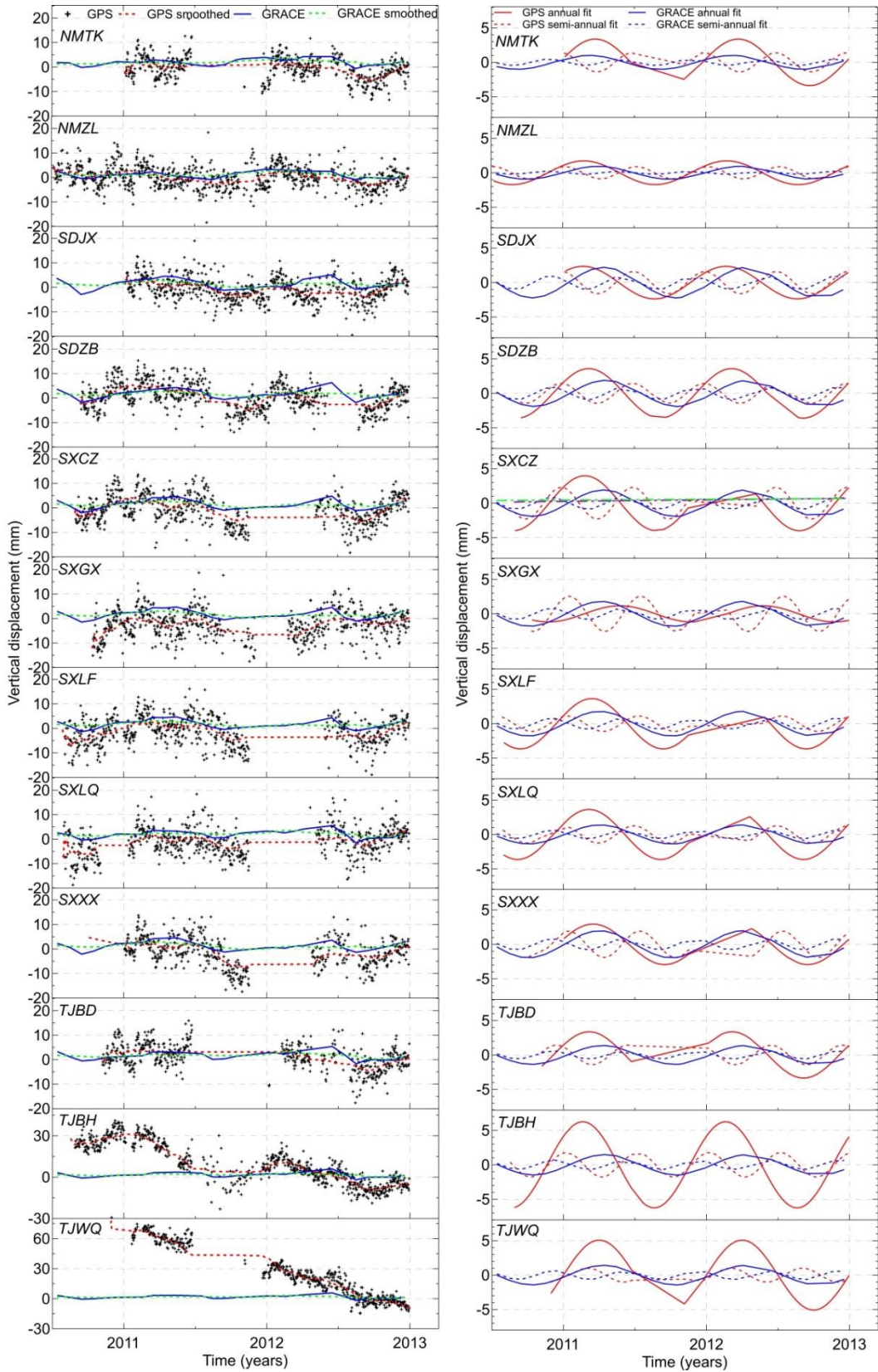
165 **Figure S2.** Compare with different  $k_n$  Love numbers.

166

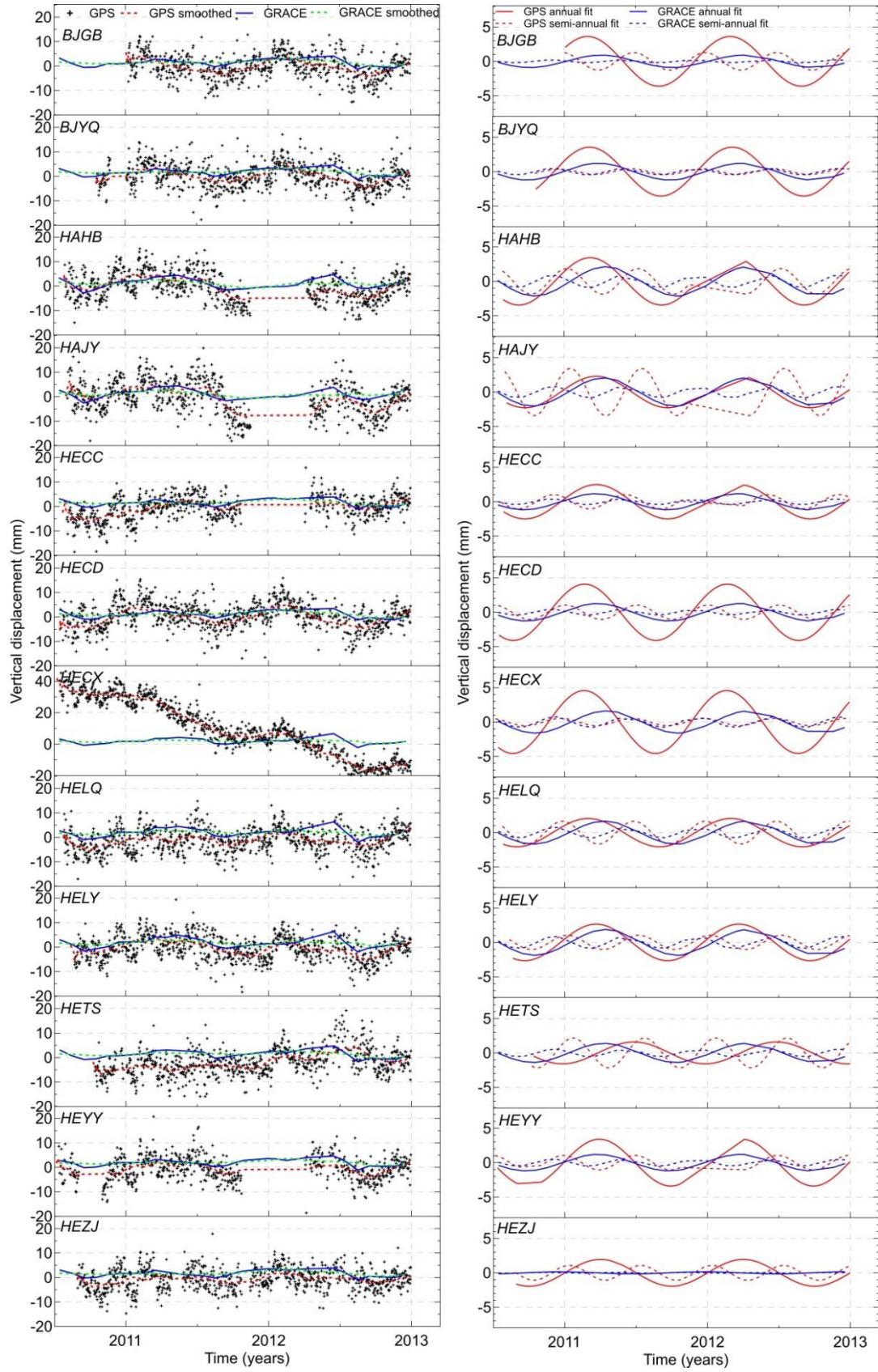


167

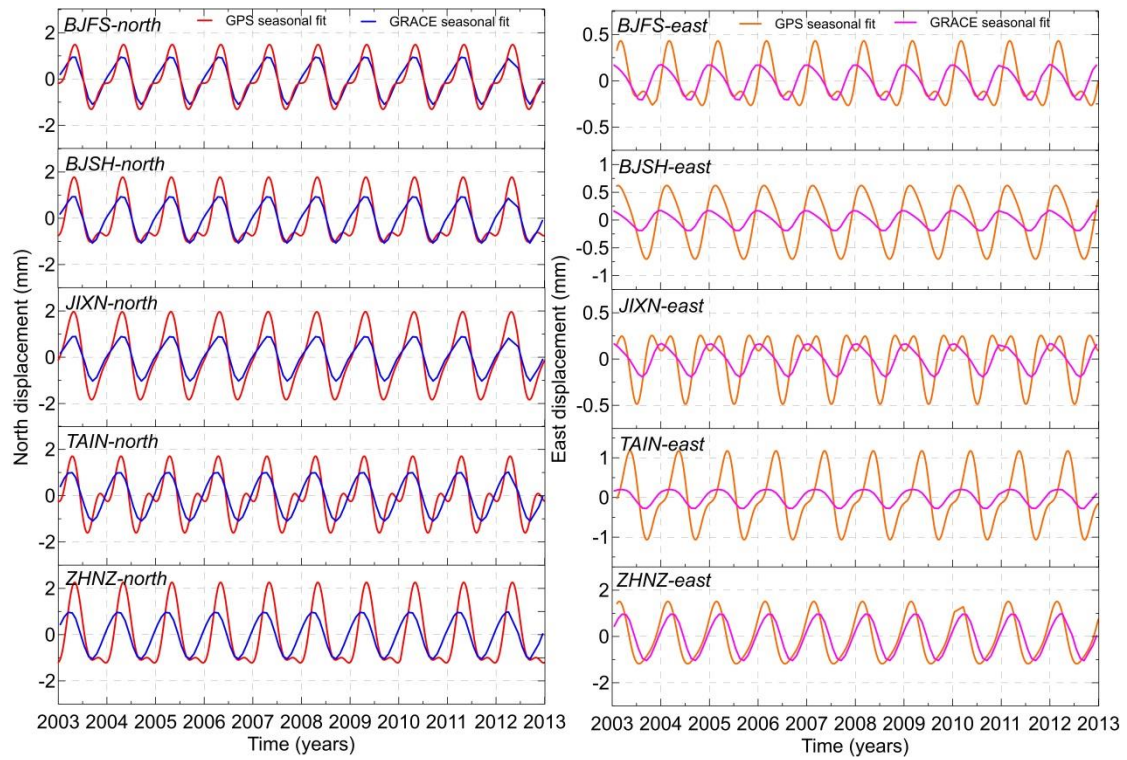
168 **Figure S3.** Comparison between GPS and GRACE-derived seasonal height variations at 24 GPS sites  
 169 from CMONOC.  
 170



to be continued



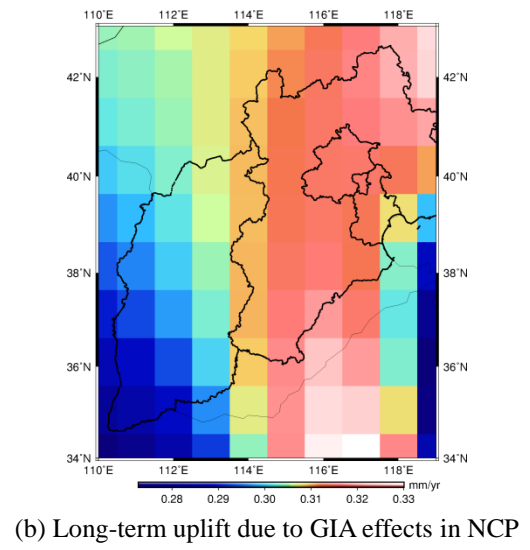
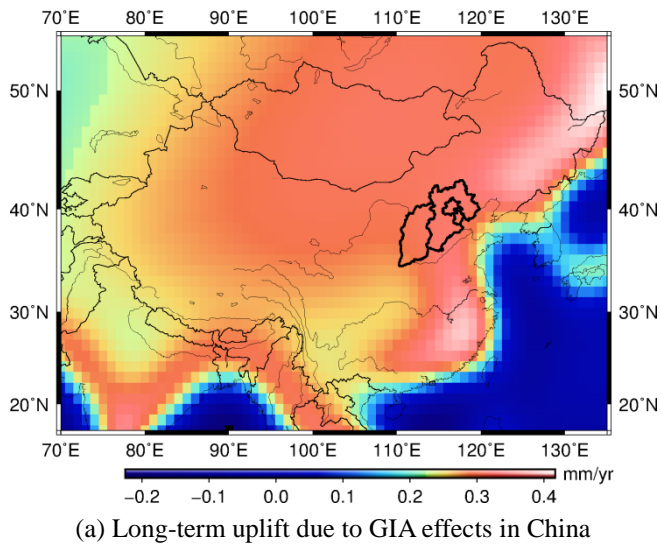
172 **Figure S4.** Comparison between GPS observed and GRACE-derived horizontal seasonal (detrended  
 173 and fit) displacements for site BJFS, BJSH, JIXN, TAIN and ZHNZ.  
 174



175

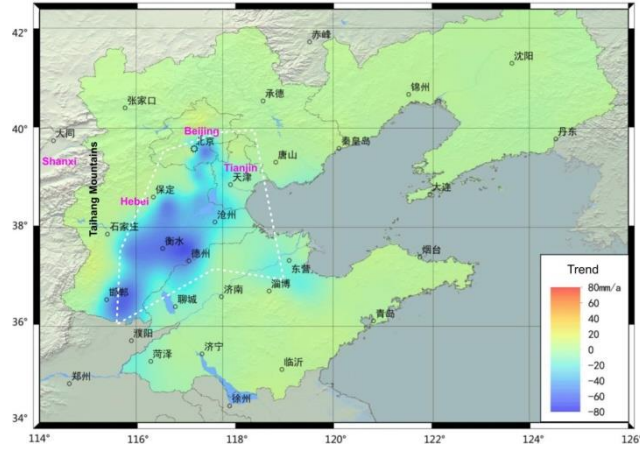
176 **Figure S5.** Long-term uplift due to GIA effects

177

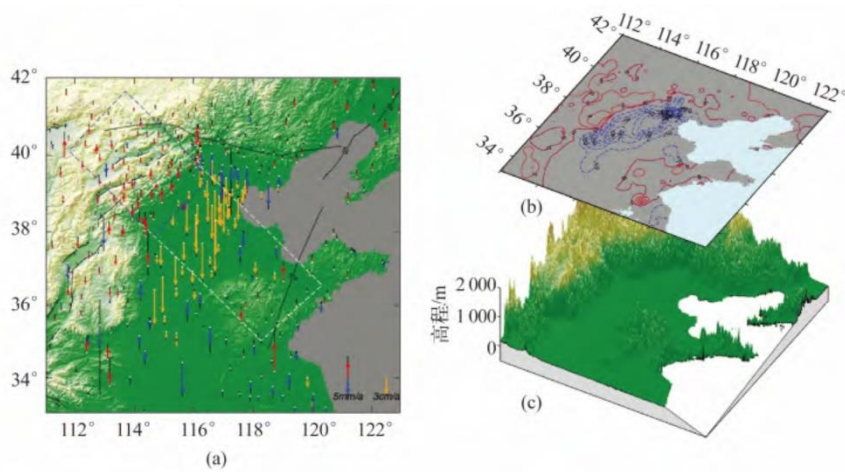


178

179 **Figure S6.** The results of vertical crust movement in the NCP from the previous study. (a) The vertical  
 180 crust movement model between 2007-2013 using GNSS GPS and leveling data, cited from MLR  
 181 (2015). (b) Vertical motion in north China with high spatial resolution, cited from Zhao et al. (2014)  
 182



(a)



(b)

183

184 **Table S1.** Seasonal amplitudes and phases fit of vertical displacements derived by GRACE and GPS  
 185 for IGS stations between before and after atmospheric and non-tidal ocean corrected.  
 186

Stations	No atmospheric and non-tidal ocean corrected				After atmospheric and non-tidal ocean corrected			
	Annual Amplitude (mm)/ Phase (days)		Semi-annual Amplitude (mm) Phase (days)		Annual Amplitude (mm)/ Phase (days)		Semi-annual Amplitude (mm) Phase (days)	
	GPS	GRACE	GPS	GRACE	GPS	GRACE	GPS	GRACE
BJFS*	3.33/337.56	3.23/311.53	1.56/54.38	0.94/61.83	2.50/40.09	1.35/359.63	1.01/90.09	0.59/71.20
BJSH*	2.75/333.79	3.11/311.81	1.04/74.57	0.86/62.91	3.25/52.75	1.25/1.00	0.68/93.97	0.50/73.76
JIXN*	3.66/314.05	3.24/310.41	1.16/67.54	0.86/63.54	2.46/32.20	1.32/359.72	0.66/81.98	0.53/73.08
TAIN*	4.65/316.75	4.18/308.41	1.71/62.57	1.22/65.95	3.31/16.44	2.07/349.43	1.48/68.35	0.99/74.27
ZHNZ*	4.14/307.37	4.76/312.86	0.75/37.63	1.14/60.31	2.48/28.18	2.24/354.76	0.36/55.63	0.86/73.54

187 \*IGS sites: the observation time between 2003 and 2013.

188



189 **Table S2.** Love numbers from Guo et al. [2004], Han and Wahr [1995].

190

Degree	Some atmospheric pressure-load			Some Love numbers			Some Love numbers
	Love numbers [Guo et al., 2004]			from Han and Wahr [1995]			from ADO1B products
$l$	$h_l$	$k_l$	$l_l$	$h_l$	$k_l$	$l_l$	$k_l$
0	-0.13206	0.00000	0.00000	-0.13273	0.00000	0.00000	0.00000
1	-0.28569	0.00000	-0.89642	-0.28796	0.00000	0.10283	0.00000
2	-0.99093	-0.60314	-0.06055	-0.99016	-0.30253	0.02388	-0.30800
3	-1.05012	-0.28787	0.05520	-1.04998	-0.19413	0.06984	-0.19500
4	-1.05281	-0.17494	0.04854	-1.05306	-0.13232	0.05841	-0.13200
5	-1.08577	-0.12889	0.03779	-1.08622	-0.10368	0.04588	-0.10300
6	-1.14331	-0.10696	0.03188	-1.14380	-0.08950	0.03832	-0.08900
7	-1.21204	-0.09478	0.02889	-1.21224	-0.08135	0.03396	-0.08200
8	-1.28335	-0.08646	0.02723	-1.28358	-0.07593	0.03126	-0.07800
10	-1.42263	-0.07595	0.02547	-1.42240	-0.06862	0.02809	-0.06820
18	-1.87337	-0.05618	0.02303	-1.87087	-0.05330	0.02364	-0.05289
32	-2.33483	-0.03979	0.01989	-2.32786	-0.03870	0.01987	-0.03875
56	-2.67593	-0.02527	0.01444	-2.66104	-0.02488	0.01423	-0.02504
100	-2.96478	-0.01443	0.00893	-2.93459	-0.01428	0.00859	-0.01461

191

192 **Table S3.** Correlation between GPS and GRACE derived seasonal variations and WRMS reduction  
 193 ratio of remove GRACE-derived seasonal deformation from GPS observed detrended height time series  
 194 (between no corrected and after atmospheric and non-tidal ocean corrected).  
 195

Stations	No atmospheric and non-tidal ocean corrected		After atmospheric and non-tidal ocean corrected	
	Correlation (%)	WRMS reduction (%)	Correlation (%)	WRMS reduction (%)
BJFS*	89.83	56.05	73.42	29.37
BJSH*	92.47	58.31	62.83	18.94
JIXN*	99.62	84.75	81.52	36.59
TAIN*	98.73	80.75	87.82	45.97
ZHNZ*	98.68	76.52	77.91	33.23
BJGB#	90.87	53.92	86.44	27.79
BJYQ#	95.63	57.30	89.14	30.38
HAHB#	98.38	77.74	79.84	37.98
HAJY#	89.70	54.28	59.30	21.59
HECC#	98.85	69.01	99.64	45.16
HECD#	85.44	48.68	85.18	25.33
HECX#	90.39	41.49	62.95	19.04
HELQ#	97.48	77.27	78.44	37.80
HELY#	96.81	69.66	86.46	47.63
HETS#	84.89	37.39	18.04	-5.08
HEYI#	99.02	58.98	94.91	35.28
HEZJ#	97.98	59.20	82.74	36.21
NMTK#	96.85	43.08	90.55	25.92
NMZL#	98.56	65.88	84.99	41.86
SDJX#	96.71	73.35	63.49	19.01
SDZB#	86.08	49.36	75.34	30.13
SXCZ#	91.37	58.64	77.93	31.36
SXGX#	83.06	18.79	8.17	-18.67
SXLF#	97.02	74.30	89.12	42.99
SXLQ#	97.96	66.11	91.85	36.22
SXXX#	95.77	68.60	81.01	38.91
TJBD#	91.49	57.02	84.68	32.39
TJBH#	68.23	27.52	61.45	13.38
TJWQ#	81.93	38.52	77.26	21.53

196 \*IGS sites: the observation time between 2003 and 2013.

197 #CMONOC sites: the observation time between 2010 and 2013.

198

199

200 **Table S4.** Seasonal amplitudes and phases, trend fit of vertical displacements derived by GRACE,  
 201 remove GLDAS-derived deformation from GRACE and GIA effects for all GPS stations.  
 202

Stations	Lat.	Lon.	Annual Amplitude (mm)		Semi-annual Amplitude (mm)		Trend Rates (mm/yr)		Trend Rates (mm/yr)
			GRACE	GRACE-GLDAS	GRACE	GRACE-GLDAS	GRACE	GRACE-GLDAS	GIA
BJFS*	39.6	115.8	1.35	0.66	0.59	0.31	0.53	0.54	0.30
BJSH*	40.2	116.2	1.25	0.68	0.50	0.26	0.48	0.49	0.30
JIXN*	40	117.5	1.32	0.66	0.53	0.29	0.46	0.50	0.30
TAIN*	36.2	117.1	2.07	0.59	0.99	0.29	0.42	0.42	0.31
ZHNZ*	34.5	113.1	2.24	0.92	0.86	0.22	0.24	0.17	0.27
BJGB#	40.6	117.1	1.25	0.70	0.45	0.25	0.43	0.44	0.30
BJYQ#	40.3	115.9	1.23	0.70	0.48	0.26	0.48	0.47	0.30
HAHB#	35.6	114.5	2.13	0.74	0.93	0.24	0.32	0.26	0.28
HAJY#	35.1	112.4	2.05	0.89	0.85	0.30	0.34	0.32	0.27
HECC#	40.8	115.8	1.17	0.76	0.42	0.23	0.44	0.41	0.30
HECD#	41	117.9	1.27	0.74	0.42	0.24	0.36	0.38	0.30
HECX#	38.4	116.9	1.62	0.66	0.78	0.39	0.54	0.61	0.30
HELQ#	38.2	114.3	1.67	0.76	0.79	0.40	0.51	0.51	0.29
HELY#	37.3	114.7	1.88	0.73	0.90	0.39	0.47	0.48	0.29
HETS#	39.7	118.2	1.39	0.68	0.57	0.31	0.43	0.49	0.29
HEYY#	40.1	114.1	1.20	0.72	0.50	0.28	0.49	0.44	0.29
HEZJ#	40.8	114.9	1.13	0.77	0.42	0.24	0.44	0.39	0.30
NMTK#	40.2	111.2	1.02	0.72	0.47	0.28	0.43	0.35	0.29
NMZL#	42.2	115.9	1.15	0.94	0.32	0.22	0.31	0.25	0.30
SDJX#	35.4	116.3	2.22	0.62	1.00	0.23	0.35	0.27	0.31
SDZB#	36.8	117.9	1.90	0.65	0.93	0.34	0.45	0.48	0.31
SXCZ#	36.2	113.1	1.93	0.85	0.88	0.37	0.41	0.38	0.28
SXGX#	36.2	111.9	1.81	0.93	0.83	0.44	0.47	0.44	0.27
SXLF#	36	111.3	1.79	0.97	0.81	0.45	0.49	0.46	0.27
SXLQ#	39.3	114	1.38	0.72	0.62	0.33	0.51	0.48	0.29
SXXX#	35.1	111.2	1.98	0.98	0.82	0.37	0.40	0.40	0.27
TJBD#	39.6	117.3	1.38	0.65	0.59	0.31	0.49	0.55	0.30
TJBH#	39	117.6	1.49	0.67	0.68	0.35	0.51	0.58	0.29
TJWQ#	39.3	117.1	1.43	0.65	0.64	0.34	0.52	0.58	0.30

203 \*IGS sites: the observation time between 2003 and 2013.

204 #CMONOC sites: the observation time between 2010 and 2013.

205